Journal of Power Sources 260 (2014) 180–185

Contents lists available at ScienceDirect

Journal of Power Sources

journal homepage: www.elsevier.com/locate/jpowsour

Low-cost CoPt alloy counter electrodes for efficient dye-sensitized solar cells

Benlin He [a], Xin Meng [a], Qunwei Tang [a,*], Pinjiang Li [b], Shuangshuang Yuan [a], Peizhi Yang [c]

[a] Institute of Materials Science and Engineering, Ocean University of China, Qingdao 266100, Shandong Province, PR China
[b] Institute of Surface Micro and Nano Materials, Xuchang University, Xuchang 461000, Henan Province, PR China
[c] Key Laboratory of Advanced Technique & Preparation for Renewable Energy Materials, Ministry of Education, Yunnan Normal University, Kunming 650092, PR China

HIGHLIGHTS

- CoPt alloy counter electrodes are fabricated by an electrodeposition method.
- The charge-transfer ability toward iodide reduction is significantly enhanced.
- A conversion efficiency of 9.59% is obtained in its DSSC.
- The strategy provides new opportunities for efficient but low-cost DSSCs.

GRAPHICAL ABSTRACT

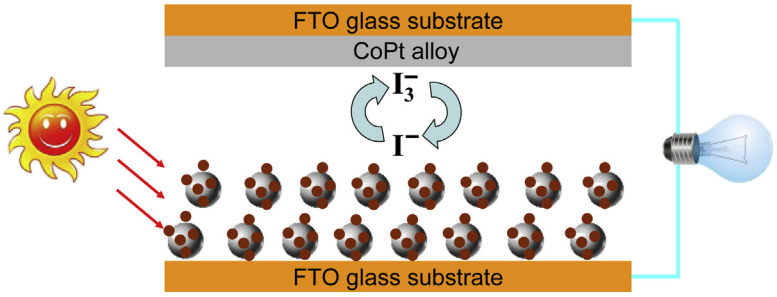

ARTICLE INFO

Article history:
Received 13 November 2013
Received in revised form
10 February 2014
Accepted 12 March 2014
Available online 19 March 2014

Keywords:
Dye-sensitized solar cell
CoPt counter electrode
Alloy
Electrodeposition

ABSTRACT

Dye-sensitized solar cell (DSSC) is a promising solution to global energy and environmental problems because of its merits on clean, low fabrication cost, relatively high power conversion efficiency, good durability, and easy assembly. However, the commercial application of DSSCs has been hindered by the high expenses of counter electrodes (CEs). With an aim of significantly enhancing the light-to-electric power conversion efficiency, here we pioneerly synthesize CoPt alloys using an electrochemically codeposition technique which are employed as CEs for efficient DSSCs. Owing to the rapid charge transfer, electrical conduction, and electrocatalysis, power conversion efficiencies of CoPt alloy CE-based DSSCs have been markedly elevated in comparison with that of the DSSC from Pt-only CE. The DSSC employing $CoPt_{0.1}$ alloy CE gives an impressive power conversion efficiency of 9.59%, which is much higher than 6.86% from conversional Pt-based DSSC. The high conversion efficiency, low cost in combination with simple preparation, and scalability demonstrates the potential use of CoPt alloy CEs in efficient DSSCs.

1. Introduction

As emerging but efficient counter electrode (CE) materials in dye-sensitized solar cells (DSSCs) [1–6], non-Pt or low-Pt alloys have been considered promising candidates for conversional Pt CEs because of their high expenses in large-scale fabrication of DSSC devices. Considering that the mission of a CE is the reduction of redox species used as a mediator in regenerating the sensitizer after electron injection in a liquid-state/quasi-solid-state DSSC, or collection of the holes from the hole-conducting material in a solid-state DSSC, conducting polymers and carbon materials as well as their composites have been employed to

* Corresponding author. Tel./fax: +86 532 66781690.
E-mail address: tangqunwei@ouc.edu.cn (Q. Tang).

http://dx.doi.org/10.1016/j.jpowsour.2014.03.035
0378-7753/

meet all of these requirements because of their low electrical resistance, reversible redox, facile synthesis, good environmental stability, and low cost. The unsatisfactory conversion efficiency promises them in a dilemma [7–11]. However, alloy CEs can also combine high electrical conductivity, superior electrocatalytic activity, and low cost. Wang et al. synthesized $Co_{0.85}Se$ and $Ni_{0.85}Se$ non-Pt alloy CEs by a low-temperature hydrothermal approach. The proposed metal selenides exhibited much higher electrocatalytic activity than Pt for the reduction of triiodide, and generated a promising power conversion efficiency of 9.40% [12]. More recently, a ternary alloy CE from $CuInGaSe_2$ alloy has been prepared by a magnetron sputtering technology, giving a conversion efficiency of 7.13% in its DSSC device [13]. However, the unfavorable power conversion efficiency is still a tremendous obstacle for alloy CEs in robust DSSCs.

To significantly enhance the power conversion efficiency of alloy-based DSSCs, herein, we develop an alternative strategy for the synthesis of a new type of low-Pt binary alloy by an electrochemical codeposition method. Regarding the efficient electrocatalyst, resultant CoPt alloy CEs demonstrate intrinsic electrocatalytic activity for the reduction of triiodide ions, rapid charge-transfer ability, and low expenses. The DSSC employing $CoPt_{0.1}$ (the atomic ratio of Co to Pt is 1: 0.1) alloy CE gives a power conversion efficiency as high as 9.59%, which is much higher than 6.86% from expensive Pt CE-based DSSC.

2. Experimental

2.1. Preparation of CoPt alloy CEs

The feasibility of this strategy was confirmed by following experimental procedures: Cleaned FTO glass substrate (sheet resistance 12 ohm $square^{-1}$, purchased from Hartford Glass Co., USA) was immersed in a reactant solution consisting of H_2PtC1_6 and $Co(NO_3)_2$. The reactant solution was prepared by dissolving H_2PtC1_6 and $Co(NO_3)_2$ in 30 ml of HCl aqueous solution (20 mmol L^{-1}) by controlling a Pt/Co (mol mol^{-1}) at 1:100, 1:50, 1:25, 1:10, 1:5. The CoPt alloy CEs were electrochemically codeposited by a potentiostatic method at a potential of −0.7 V and a deposition time of 200 s.

2.2. Assembly of DSSCs

A layer of TiO_2 nanocrystal anode film with a thickness of 10 μm was prepared by a sol-hydrothermal method. Resultant anodes were further sensitized by immersing into a 0.25 mM ethanol solution of N719 dye ([cis-di(thiocyanato)-N,N′-bis(2,2′-bipyridyl-4-carboxylic acid)-4-tetrabutylammonium carboxylate]). The DSSC was fabricated by sandwiching redox electrolyte between dye-sensitized TiO_2 anode and FTO supported CoPt alloy CEs. A redox electrolyte consisted of 100 mM of tetraethylammonium iodide, 100 mM of tetramethylammonium iodide, 100 mM of tetrabutylammonium iodide, 100 mM of NaI, 100 mM of KI, 100 mM of LiI, 50 mM of I_2, and 500 mM of 4-tert-butyl-pyridine in 50 ml acetonitrile.

2.3. Electrochemical characterizations

The electrochemical performances were recorded on a conventional CHI660E setup comprising an Ag/AgCl reference electrode, a CE of platinum sheet, and a working electrode of FTO glass supported CoPt alloy. The cyclic voltammetry (CV) curves were recorded from −0.6 to +1.4 V and back to −0.6 V. Before the measurement, the supporting electrolyte consisting of 50 mM M LiI, 10 mM I_2, and 500 mM $LiClO_4$ in acetonitrile was degassed using nitrogen for 10 min. Electrochemical impedance spectroscopy (EIS) measurements were also carried out on the CHI660E Electrochemical Workstation in a frequency range of 0.01 Hz ~ 10^6 kHz and an ac amplitude of 10 mV at room temperature. The resultant impedance spectra were analyzed using the Z-view software. The resultant impedance spectra were analyzed using the Z-view software. Tafel polarization curves were recorded on the same Workstation by assembling symmetric cell consisting of FTO/CoPt alloy|redox electrolyte|FTO/CoPt alloy.

2.4. Photovoltaic measurements

The photovoltaic test of the DSSC was carried out by measuring the current–voltage (J–V) characteristic curves using an Electrochemical Workstation (CHI660E, Shanghai Chenhua Device Company, China) under irradiation of a simulated solar light from a 100 W Xenon arc lamp (XQ-500 W, Beijing Trusttech Co., Ltd) in ambient atmosphere. The incident light intensity was calibrated using a FZ-A type radiometer from Beijing Normal University Photoelectric Instrument Factory to control it at 100 mW cm^{-2} (AM 1.5).

2.5. Other characterizations

The morphology of the $CoPt_{0.1}$ alloy CE was observed with a scanning electron microscope (SEM, S4800). The XRD data were collected in a scan mode with a scanning speed of 10° min^{-1} in the 2θ range between 10 and 80°. The compositions of the alloy CEs were detected by inductively coupled plasma-atomic emission spectra (ICP-AES). Prior to ICP measurements, the alloy CEs were immersed in concentration nitric acid to dissolve the FTO glass substrate thoroughly.

3. Results and discussion

The CoPt alloys were subjected to XRD measurements. As shown in Fig. 1a, XRD results indicate that the as-prepared samples consist of CoPt (fm-3m, PDF# 65-8968) and bared FTO layer (PDF# 46-1088). The compositions of the alloys on FTO glass substrate were determined by ICP-AES equipment. The results display that the atomic ratios of $CoPt_{0.01}$, $CoPt_{0.02}$, $CoPt_{0.04}$, $CoPt_{0.1}$, and $CoPt_{0.2}$ are 1.000: 0.009, 1.000: 0.019, 1.000: 0.038, 1.000: 0.097, and 1.000: 0.196, respectively. The measured atomic ratios are close to the stoichiometry of $CoPt_{0.01}$, $CoPt_{0.02}$, $CoPt_{0.04}$, $CoPt_{0.1}$, and $CoPt_{0.2}$, therefore, the chemical formulas of the alloy CEs can be expressed according to their stoichiometric ratios. SEM photograph in Fig. 1b suggests a higher surface coverage and loading on FTO substrate. The relatively loose structure between aggregations provides channels for triiodide ions across the alloy layer [14,15]. From energy-dispersive X-ray spectrum, as shown in Fig. 1c, Pt and Co elements as well as the elements from FTO substrate are detected, indicating that Pt and Co have been successfully codeposited on FTO glass substrate.

Fig. 2 shows J–V curves of the DSSCs using CoPt alloy and Pt as CEs. The detailed photovoltaic parameters from the J–V curves are summarized in Table 1. The DSSC with $CoPt_{0.1}$ CE yields a remarkable η of 9.59%, J_{sc} of 17.92 mA cm^{-2}, V_{oc} of 0.735 V, and FF of 0.728, while the DSSC with pure Pt CE (300–400 μm in thickness, purchased from Dalian HepatChroma SolarTech Co., Ltd) gives a η of 6.86%, J_{sc} of 14.51 mA cm^{-2}, V_{oc} of 0.715 V, and FF of 0.661. The recorded V_{oc} in all J–V curves are close because the similar photoanodes are employed, whereas there is a large difference in J_{sc}. J_{sc} is a parameter reflecting the density of electrons from excited dyes to conduction band of TiO_2

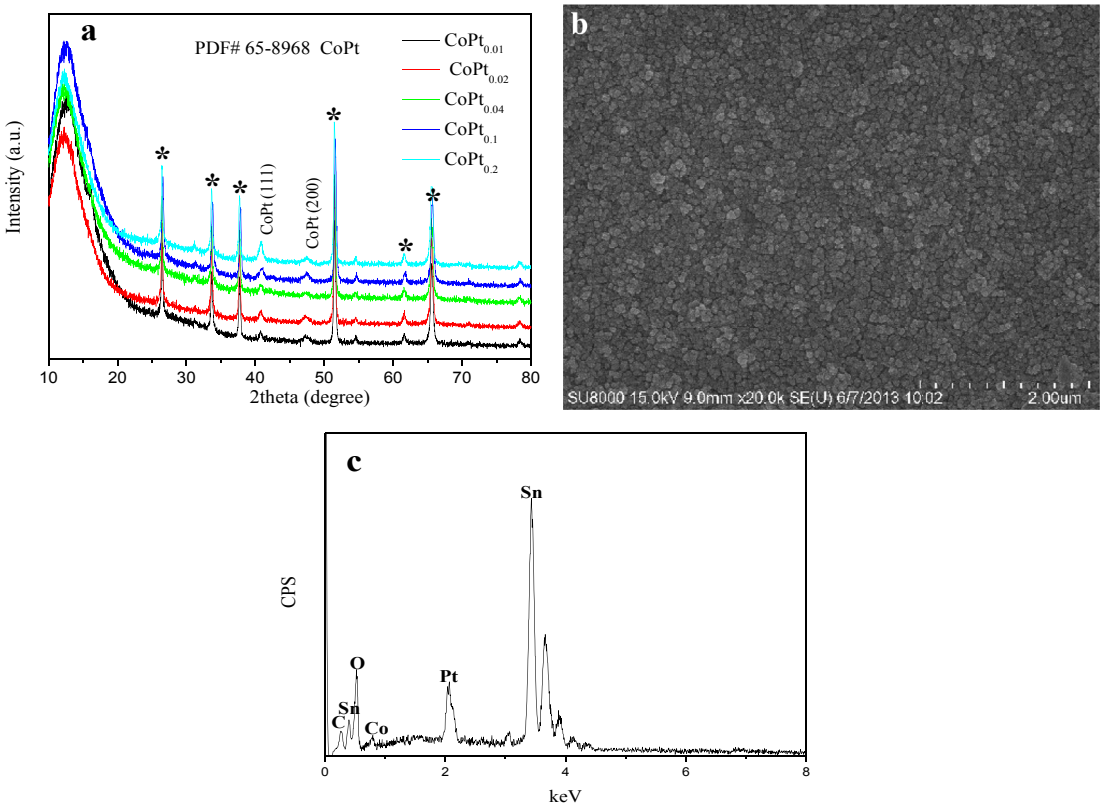

Fig. 1. (a) XRD patterns of varied CoPt alloy CEs and (b) SEM image of $CoPt_{0.1}$ alloy CE. (c) Energy-dispersive X-ray spectrum of $CoPt_{0.1}$ alloy CE.

nanocrystallines. Once an N719 molecule releases an electron, it can be reduced by I^-/I_3^- redox species which are subsequently reduced by alloy CE. Therefore, the J_{sc} values of the DSSC devices are of highly dependent on electrocatalytic activity of CEs. From Fig. 3a, the $CoPt_{0.1}$ alloy CE exhibits the best electrocatalytic activity toward I^-/I_3^- redox couples, revealing that the $CoPt_{0.1}$ alloy CE has the highest J_{sc}. The recorded efficiencies from CoPt alloy CEs are impressive for low-Pt electrocatalysts in DSSCs. To the best of our knowledge, the recorded power conversion efficiency is in a very high level for I^-/I_3^- redox couple based DSSCs with low-Pt or non-Pt CEs under AM1.5G simulated solar light (100 mW cm^{-2}) [16–18].

In the cyclic voltammograms (CVs), as shown in Fig. 3a, the peak positions of the CoPt alloys are very similar to that of Pt electrode, showing that CoPt alloys have a similar electrocatalytic function to the Pt electrode. Furthermore, CoPt alloy CEs have higher current densities, suggesting larger active surfaces [19,20]. Considering that the task of CE is the reduction of redox species used as a mediator in regenerating the sensitizer after electron injection in a liquid-state DSSC. The electroreduction reaction of $I_3^- + 2e \rightarrow 3\ I^-$ can be employed to elevate the electrocatalytic activity of CoPt alloy CEs. Among various CoPt alloys, $CoPt_{0.1}$ is the most efficient electrocatalyst. The employment of alloy CE in DSSCs is a pioneering work, however, that is relatively popular in fuel cells [21,22]. Xu et al.

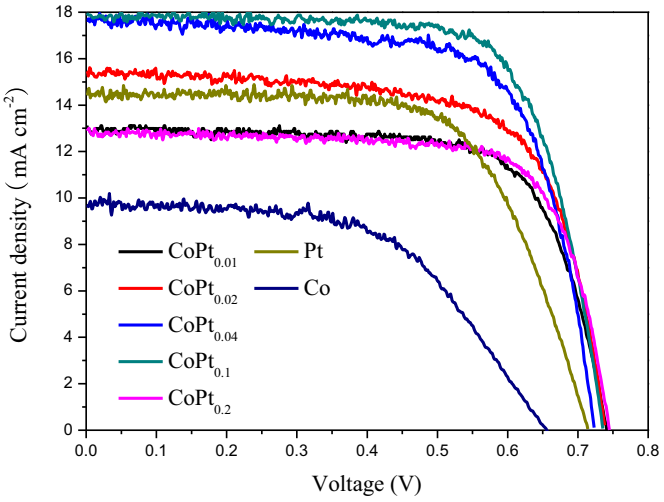

Fig. 2. Characteristic *J–V* curves of DSSCs from varied CEs.

Table 1
Photovoltaic parameters of DSSCs with varied CEs and the simulated data from EIS spectra.[a]

CEs	η (%)	V_{oc} (V)	*FF*	J_{sc} (mA cm^{-2})	R_s (Ω cm^2)	R_{ct} (Ω cm^2)	*W* (Ω cm^2)
$CoPt_{0.01}$	6.93	0.740	0.723	12.95	15.48	4.50	1.23
$CoPt_{0.02}$	7.84	0.738	0.690	15.39	14.78	4.18	0.90
$CoPt_{0.04}$	8.95	0.723	0.700	17.68	15.14	2.19	0.58
$CoPt_{0.1}$	9.59	0.735	0.728	17.92	14.51	1.44	1.09
$CoPt_{0.2}$	7.01	0.745	0.729	12.91	14.06	1.45	0.58
Pt	6.86	0.715	0.661	14.51	23.40	13.00	1.23
Co	3.64	0.655	0.572	9.71	–	–	–

[a] V_{oc}: open-circuit voltage; J_{sc}: short-circuit current density, *FF*: fill factor; η: power conversion efficiency; R_s: ohmic internal resistance; R_{ct}: charge-transfer resistance; *W*: diffusion impedance.

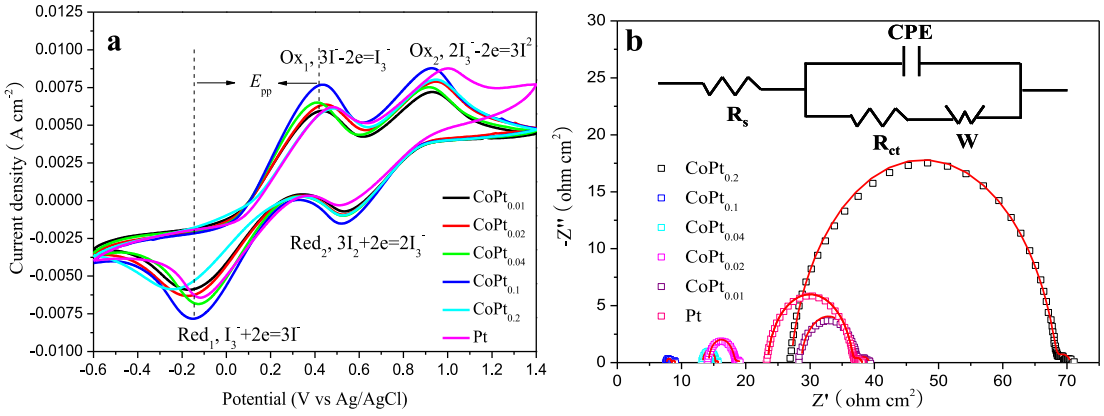

Fig. 3. (a) CV curves and (b) EIS spectra of CoPt alloy CEs for I^-/I_3^- redox species. The CV curves were recorded at a scan rate of 50 mV s^{-1}. The lines express fit results for corresponding EIS data, and the inset gives the equivalent circuit.

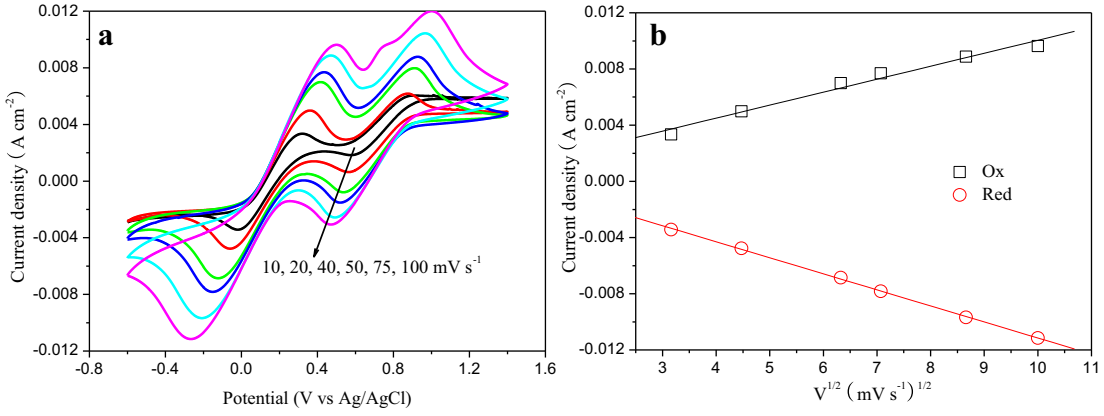

Fig. 4. (a) CV curves of $CoPt_{0.1}$ alloy CE for I^-/I_3^- redox species at different scan rates (from inner to outer: 10, 20, 40, 50, 75, and 100 mV s^{-1}), and (b) relationship between peak current density and square root of scan rates.

demonstrated that alloying of Co can effectively tune the electron structure of Pt because the alloying of Co and Pt can lower the d-band center of Pt [23]. It is expected that the molar amount of Co/Pt at 1/0.1 can bring most favorable electronic perturbation for Pt electron structure. Similar promotion effect has also been found in NiPt alloys [24]. Notably, the CoPt alloy CEs decrease the peak-to-peak separation (E_{pp}), suggesting an enhanced electroreductive behavior to I^-/I_3^- redox. Moreover, the ratio of $J_{ox1}/|J_{red1}|$ is a parameter to elevate the reversibility of the redox reaction toward I^-/I_3^- [25]. The obtained value from $CoPt_{0.1}$ alloy CE (0.992) is closer to 1.0 that $CoPt_{0.01}$ (1.014), $CoPt_{0.02}$ (1.015), $CoPt_{0.04}$ (0.959), $CoPt_{0.2}$ (1.057), and Pt (0.965), indicating a more reversible redox reaction for $I_3^- \leftrightarrow I^-$. The rapid recovery of iodides to their ground state facilitates the participation in subsequent circles and improves the long-term stability. Randles-Sevcik theory is employed To elucidate the diffusion of iodide in CE [26], giving diffusion coefficients for $CoPt_{0.01}$, $CoPt_{0.02}$, $CoPt_{0.04}$, $CoPt_{0.1}$, $CoPt_{0.2}$, and Pt CEs of 1.21×10^{-5}, 1.41×10^{-5}, 1.61×10^{-5}, 2.10×10^{-5}, 1.19×10^{-6}, and 1.44×10^{-5} cm^{-2} s^{-1}, respectively. Results indicate that the CoPt alloys can accelerate the diffusion kinetics of iodide species within CEs.

A standard criterion to determine the charge-transfer mechanism is recording the CV curves at various scan rates (Fig. 4a): peak current densities plotted against square roots of scan rates for the $CoPt_{0.1}$ alloy CE. The linearity of the peak current densities with the square root of scan rates in Fig. 4b indicates that charge transfer in the redox step is controlled by the diffusion of charges in the films as described by the empirical Randles-Sevcik theory [27]:

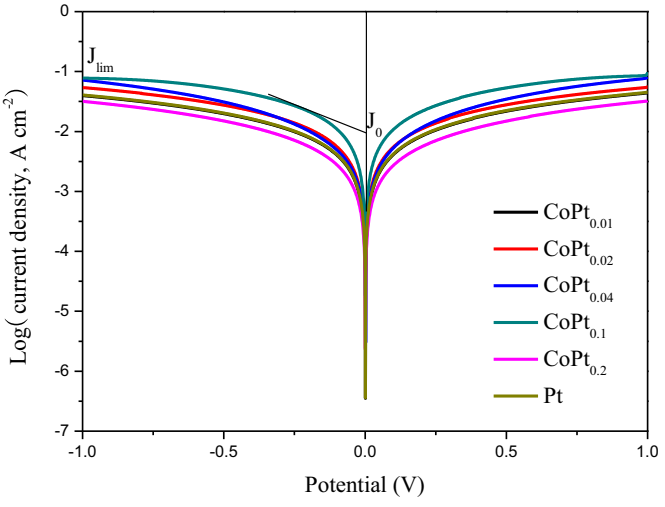

Fig. 5. Tafel polarization curves of symmetrical cells fabricated with Pt and CoPt alloy CEs that are same as the ones used in EIS experiments.

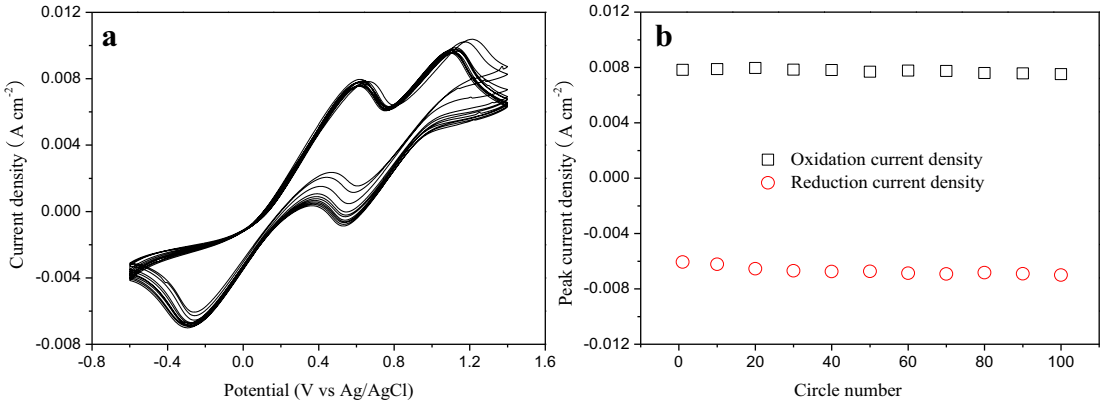

Fig. 6. (a) CV curves of 100 cycles using $CoPt_{0.1}$ as working electrode at a scan rate of 50 mV s^{-1}. (b) The peak current density stability as a function of cycle.

$$i_p = \left(2.69 \times 10^5\right) n^{3/2} A D_{ct}^{1/2} \nu^{1/2} C_0 \quad (1)$$

where D_{ct} is the charge transport diffusion coefficient and C_0 is the concentration of electroactive sites. The dependence of the peak current densities on scan rate is determined by $D_{ct}\tau/d^2$, where τ is the experimental time scale (the time for the potential to traverse the wave) and d is the film thickness. $D_{ct}\tau/d^2 >> 1$ means charger-transfer rate is significantly high compared to the experimental time, giving a linear fitting of peak current density *vs* scan rate. However, peak current density is directly proportional to square root of scan rate at $D_{ct}\tau/d^2 << 1$, giving a much smaller charge-transfer rate.

Tafel polarization was carried out and presented in Fig. 5 by recording on the symmetrical cells to reveal the interfacial charge-transfer properties at the CE/electrolyte interface. The larger slope for the anodic or cathodic branch indicates a higher exchange current density (J_0) on the electrode and better catalytic activity toward triiodide reduction. Apparently, the calculated J_0 also follows an order of $CoPt_{0.1} > CoPt_{0.04} > CoPt_{0.02} > Pt > CoPt_{0.01} > CoPt_{0.2}$, which match the order of R_{ct}. The elevated J_0 is the result of rapid charge-transfer [14]. The intersection of the cathodic branch with the *Y*-axis can be considered as the limiting diffusion current density (J_{lim}), which determined by the diffusion properties of the redox couple and the CE catalysts. One can see that the J_{lim} also follows an order of $CoPt_{0.1} > CoPt_{0.04} > CoPt_{0.02} > Pt > CoPt_{0.01} > CoPt_{0.2}$.

CV curves of 100 cycles have been scanned to determine the continuous electrocatalysis of triiodides by $CoPt_{0.1}$ alloy CE as shown in Fig. 6. No apparent decrease in peak current density from redox reaction of triiodides is observed, indicating that the $CoPt_{0.1}$ alloy CE can consistently reduce the triiodides into iodides, which is desirable for stable DSSCs.

4. Conclusions

In summary, we have demonstrated that electrochemical codeposition is an effective strategy in fabricating low-cost CoPt alloy CEs and enhancing the photovoltaic performances of DSSCs. $CoPt_{0.1}$ alloy exhibits amazing electrocatalytic activity for the reduction of triiodide ions. The DSSC from $CoPt_{0.1}$ alloy CE provides an impressive power conversion efficiency of 9.59% in comparison with that of 6.86% from pure Pt CE. The research presented here is far from being optimized but these profound advantages along with low-cost synthesis and scalable materials promise the new alloy CEs to be strong candidates in robust DSSCs.

Acknowledgments

The authors gratefully acknowledge Ocean University of China for providing Seed Fund to this project, and Fundamental Research Funds for the Central Universities (201313001, 201312005), Shandong Province Outstanding Youth Scientist Foundation Plan (BS2013CL015), Doctoral Fund of Ministry of Education of China (20130132120023), Shandong Provincial Natural Science Foundation (ZR2011BQ017), Research Project for the Application Foundation in Qingdao (13-1-4-198-jch), and Natural Science Foundation of China (U1037604).

References

[1] B. O'Regan, M. Grätzel, Nature 353 (1991) 737–740.
[2] U. Bach, D. Lupo, P. Comte, J.E. Moser, F. Weissortel, J. Salbeck, M. Grätzel, Nature 395 (1998) 583–585.
[3] M. Grätzel, Nature 414 (2001) 338–344.
[4] J.H. Wu, Y. Li, Q.W. Tang, G.T. Yue, J.M. Lin, M.L. Huang, L.J. Meng, Sci. Rep. 4 (2014) 4028.
[5] B.L. He, Q.W. Tang, J.H. Luo, Q.H. Li, X.X. Chen, H.Y. Cai, J. Power Sources 256 (2014) 170–177.
[6] B.L. He, Q.W. Tang, M. Wang, C.Q. Ma, S.S. Yuan, J. Power Sources 256 (2014) 8–13.
[7] H. Wang, K. Sun, F. Tao, D.J. Stacchiola, Y.H. Hu, Angew. Chem. Int. Ed. 52 (2013) 9210–9214.
[8] Q.W. Tang, H.Y. Cai, S.S. Yuan, X. Wang, J. Mater. Chem. A 1 (2013) 317–323.
[9] Q.H. Li, J.H. Wu, Q.W. Tang, Z. Lan, P.J. Li, J.M. Lin, L.Q. Fan, Electrochem. Commun. 10 (2008) 1299–1302.
[10] Q. Tai, B. Chen, F. Guo, S. Xu, H. Hu, B. Sebo, X.Z. Zhao, ACS Nano 5 (2011) 3795–3799.
[11] J. Han, H. Kim, D.Y. Kim, S.M. Jo, S.Y. Jang, ACS Nano 4 (2010) 3503–3509.
[12] F. Gong, H. Wang, X. Xu, G. Zhou, Z.S. Wang, J. Am. Chem. Soc. 134 (2012) 10953–10958.
[13] X.Y. Cheng, Z.J. Zhou, Z.L. Hou, W.H. Zhou, S.X. Wu, Sci. Adv. Mater. 5 (2013) 1193–1198.
[14] W. Zeng, G. Fang, X. Wang, Q. Zheng, B. Li, H. Huang, H. Tao, N. Liu, W. Xie, X. Zhao, D. Zou, J. Power Sources 229 (2013) 102–111.
[15] S.H. Park, B.K. Kim, W.J. Lee, J. Power Sources 239 (2013) 122–127.
[16] L.H. Chang, C.K. Hsieh, M.C. Hsiao, J.C. Chiang, P.I. Liu, K.K. Ho, et al., J. Power Sources 222 (2013) 518–525.
[17] W. Zeng, G. Fang, T. Han, B. Li, N. Liu, D. Zhao, et al., J. Power Sources 245 (2014) 456–462.
[18] W. Cho, D. Song, Y.G. Lee, H. Chae, Y.R. Kim, Y.B. Pyun, et al., J. Mater. Chem. A 1 (2013) 233–236.
[19] M.K. Wang, A.M. Anghel, B. Marsan, N.C. Ha, N. Pootrakulchote, S.M. Zakeeruddin, M. Grätzel, J. Am. Chem. Soc. 131 (2009) 15976–15977.
[20] Z. Huang, X.Z. Liu, K.X. Li, D.M. Li, Y.H. Luo, H. Li, W.B. Song, L.Q. Chen, Q.B. Meng, Electrochem. Commun. 9 (2007) 596–598.
[21] Y. Shao, J. Liu, Y. Wang, Y. Lin, J. Mater. Chem. 19 (2009) 46–59.
[22] A. Morozan, B. Jousselme, S. Palacin, Energy Environ. Sci. 4 (2011) 1238–1254.

[23] C. Xu, J. Hou, X. Pang, X. Li, M. Zhu, B. Tang, Int. J. Hydrogen Energy 37 (2012) 10489–10498.
[24] G.J. Wang, Y.Z. Gao, Z.B. Wang, C.Y. Du, J.J. Wang, G.P. Yin, J. Power Sources 195 (2010) 185–189.
[25] H. Tributsch, Coord. Chem. Rev. 248 (2004) 1511–1530.
[26] T. Daeneke, A.J. Mozer, T.H. Kwon, N.W. Duffy, A.B. Holmes, U. Bach, L. Spiccia, Energy Environ. Sci. 5 (2012) 7090–7099.
[27] Y.M. Xiao, J.Y. Lin, S.Y. Tai, S.W. Chou, G.T. Yue, J.H. Wu, J. Mater. Chem. 22 (2012) 19919–19925.